On the Realization of Resistively Matched Three-Ports and the Ramp-Waveform Responses of Resistive, Signal-Split Three-Port Transmission-Line Networks

Iwata Sakagami, *Member, IEEE,* and Akihiro Kaji

Abstract— **Three-port networks consisting of three transmission lines and three branching resistors at a junction, for the conditions of TEM wave propagation and lossless lines, are discussed. This discussion entails the following: 1) The matching conditions for the resistive three-port are modeled by scattering matrices. 2) As transmission lines of unequal length are used, the network transfer functions are derived for three different delay variables. These functions are obtained in a matrix form after their expansions with respect to these variables are derived. As a consequence, output waveforms can be calculated from the network transfer functions or their expansions. This method of expansion is superior to the conventionally used lattice diagram for analyzing high-speed logic circuits and designing their interconnections. 3) Three characteristics of output waveforms are discussed. 4) Ideal networks that furnish the same output waveforms as their inputs and practical networks that have parameters as close as possible to the ideal are described. 5) Examples of networks that keep the ringing of output waveforms within given tolerances, from the first arriving wave to the steady state, are presented. 6) Finally, this paper concludes with a discussion of power dissipation.**

I. Introduction

THE DEVELOPMENT of high-speed logic circuits has led to a need for higher-speed pulse techniques. Progress has been made, but there are still some problems with the equalization of distorted pulse waveforms [1], [2] and with the suppression of multiple reflections (reflected waves), which propagate on printed transmission lines between connecting points and mismatched terminals, such as the input ports of high-impedance logical circuits [3]–[5]. These multiple reflections also arise at the junction of three transmission lines when the signals on a transmission line are split. This results in distorted waveforms, an increase in the effective rise time, and false triggerings.

The time-domain behavior of distributed transmission-line networks has been studied in [6]–[10]. This paper discusses the problems of a transmission-line network with one branch, as treated earlier in [11]–[14], and presents a method for obtaining output waveforms similar (within given tolerances) to the input waveform. Our discussion proceeds as follows:

Manuscript received April 10, 1991; revised June 11, 1992.

The authors are with the Department of Electrical and Electronic Engineering, Muroran Institute of Technology, Mizumoto-cho, Muroran-shi, Hokkaido, 050 Japan.

IEEE Log Number 9204477.

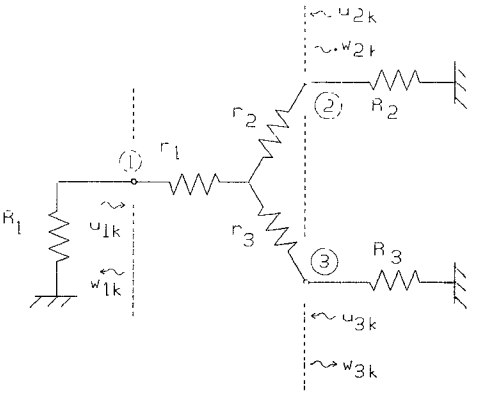

Fig. 1. Circuit representation of a resistive three-port.

1) The realization of a resistively matched three-port (Fig. 1) is discussed, and the non-negative region of this realization is presented for the case of arbitrary load resistors (Fig. 2).
2) The network transfer functions of the circuit in Fig. 3, as well as their expansions, are derived for the analysis of output responses and circuit design; each term of the expansions corresponds to an individual reflection, e.g. the first arriving wave, the second arriving wave, and so on.
3) Characteristics of the output response—especially the steady-state voltage, the monotonic increment, and the effective delay time—are examined.
4) Ideal networks are suggested, i.e., networks whose output waveforms are identical to the input waveforms, and where no reflections are created. However, as these ideal networks cannot be realized physically (i.e., they are in the negative region of realization), networks that mimic as closely as possible an ideal response are presented.
5) Limitations on the range of the voltage of the first arriving wave (i.e., the first arriving voltage) are discussed with regard to the quasi-ideal networks discussed above.
6) Finally, the power dissipation in the circuits of interest is discussed.

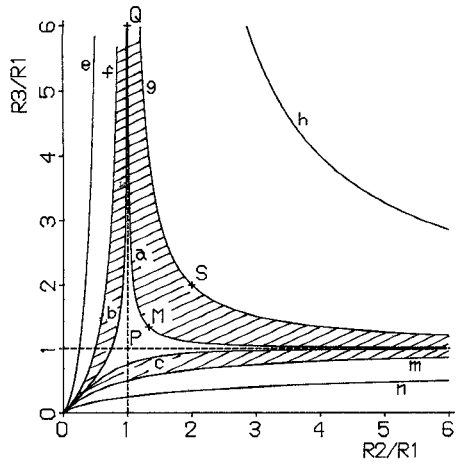

Fig. 2. The realization region of resistively matched three-ports. The clear area inside the hatched area represents $r_1, r_2, r_3 \geq 0$. The region $r_1, r_2, r_3 \geq 0$ plus the hatched area represents $0 < s_{12}, s_{13}, s_{23} < 1$.

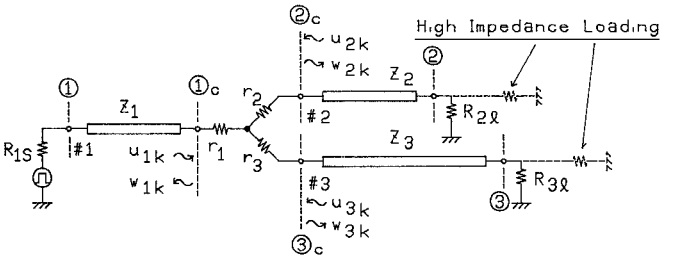

Fig. 3. A three-port consisting of transmission lines and branching resistors.

II. The Realization of Resistively Matched Three-Ports

Fig. 1 depicts a resistively matched three-port where

$R_1, R_2, R_3$are load resistors at ports $1_c, 2_c, 3_c$, respectively;

r_1, r_2, r_3 are branching resistors;

u_{1k}, u_{2k}, u_{3k} are incident voltage waves; and

w_{1k}, w_{2k}, w_{3k} are reflected voltage waves.

The voltage wave matrix $[\boldsymbol{T}]$ of Fig. 1 is given by

$$\begin{bmatrix} w_{ik} \\ w_{2k} \\ w_{3k} \end{bmatrix} = \begin{bmatrix} \Gamma_{11} & T_{21} & T_{31} \\ T_{12} & \Gamma_{22} & T_{32} \\ T_{13} & T_{23} & \Gamma_{33} \end{bmatrix} \begin{bmatrix} u_{1k} \\ u_{2k} \\ u_{3k} \end{bmatrix}$$

or $\boldsymbol{w}_k = [\boldsymbol{T}]\boldsymbol{u}_k$. (1)

The subscripts $[\boldsymbol{T}]$ are not those conventionally used. However, this notation is useful as it represents the direction of the signals and makes it easier to visualize their flow, as shown in Fig. 4. For instance, T_{12} represents a voltage-transmission coefficient from ports 1_c to 2_c. In general, the elements in $[\boldsymbol{T}]$ are given by

$$\Gamma_{ii} = [(r_i - R_i)(X_j + X_k) + X_j X_k]/\Delta_R \quad (2a)$$

$$T_{ij} = 2R_j X_k/\Delta_R \quad (2b)$$

where Γ_{ii} is the coefficient of voltage reflection at port i_c; $X_i = r_i + R_i$; $\Delta_R = X_1X_2 + X_2X_3 + X_3X_1$ and $i, j,$ and $k = 1, 2, 3$, respectively. The scattering matrix can be written as

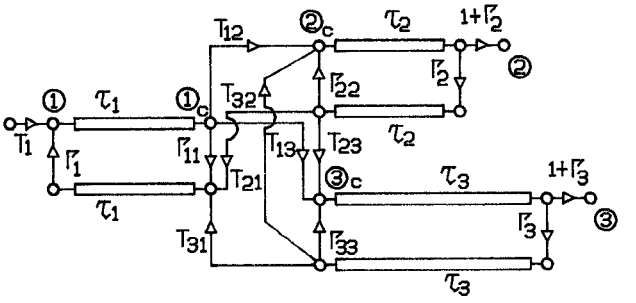

Fig. 4. A signal flow graph (SFG) for the circuit of Fig. 3.

$$[\boldsymbol{S}] = [\sqrt{\boldsymbol{R}}]^{-1}[\boldsymbol{T}][\sqrt{\boldsymbol{R}}] \quad (3)$$

where $[\sqrt{\boldsymbol{R}}] = \text{diag}\,(\sqrt{R_1}, \sqrt{R_2}, \sqrt{R_3})$. Therefore, $S_{ii} = \Gamma_{ii}$ and $S_{ij} = A_{ij}T_{ji}$. Obviously, $T_{ij} \neq T_{ji}$ at $R_i \neq R_j$, but $S_{ij} = S_{ji} = 2B_{ij}X_k/\Delta_R$ (where $A_{ij} = \sqrt{R_j/R_i}$ and $B_{ij} = \sqrt{R_iR_j}$).

For equal load resistors, it has been known that the matching conditions at all three ports are given by $r_i = R_0/3$, where $R_0 = R_i$, $i = 1, 2, 3$ [2], [11]. This ensures that at least one realization exists, and provides for the following assumption:

$$[\boldsymbol{S}] = \begin{bmatrix} 0 & s_{12} & s_{13} \\ s_{12} & 0 & s_{23} \\ s_{13} & s_{23} & 0 \end{bmatrix}. \quad (4)$$

Therefore, a problem that remains is to determine the realization regions of r_i for arbitrary load resistors. In the treatment of matching networks that follows, s_{ij}'s will represent the elements of a scattering matrix. In general,

$$[\boldsymbol{Z}] = [\sqrt{\boldsymbol{R}}](\boldsymbol{E} + [\boldsymbol{S}])(\boldsymbol{E} - [\boldsymbol{S}])^{-1}[\sqrt{\boldsymbol{R}}] \quad (5)$$

where $[\boldsymbol{Z}]$ is the impedance matrix and $\boldsymbol{E}$ is the unit matrix. For the case of ports i and j,, (5) yields

$$[\boldsymbol{Z}]_{ij} = \frac{1}{(1 - s_{ij}^2)} \begin{bmatrix} R_i(1 + s_{ij}^2) & 2B_{ij}s_{ij} \\ 2B_{ij}s_{ij} & R_j(1 + s_{ij}^2) \end{bmatrix}. \quad (6)$$

When the resistance $X_k = r_k + R_k$ is grounded, the network shown in Fig. 1 is regarded as a T-type two-port with respect to ports i and $j (i, j \neq k)$. Therefore, the impedance matrix of this two-port is given by [15]

$$[\boldsymbol{Z}]_{ij} = \begin{bmatrix} r_i + X_k & X_k \\ X_k & r_j + X_k \end{bmatrix} \quad (7)$$

From (6) and (7), the desirable resistance for the branching resistors r_i, for all three ports to be matched to the load resistors, can be obtained as follows:

$$r_i = R_i(s_{ij}^2 - 2A_{ij}s_{ij} + 1)/(1 - s_{ij}^2) \quad (8a)$$

$$r_j = R_j(s_{ij}^2 - 2A_{ji}s_{ij} + 1)/(1 - s_{ij}^2) \quad (8b)$$

$$r_k = R_k\left[\left(s_{ij}^2 + \frac{2B_{ij}s_{ij}}{R_k} - 1\right)\right]\Big/(1 - s_{ij}^2). \quad (8c)$$

Equations (8a) and (8b) satisfy the input match at ports i and j, respectively. For the input match at port k, it is necessary

TABLE I
NUMERICAL EXAMPLES OF THREE -PORTS

	Point S(2,2)	Point M(4/3,4/3)	Point Q(1,6)
R_i	$R_1 = 1$ $R_2 = R_3 = 2$	$R_1 = 1$ $R_2 = R_3 = \frac{4}{3}$	$R_1 = R_2 = 1$ $R_3 = 6$
r_i	$r_1 = -1$ $r_2 = r_3 = 2$	$r_1 = 0$ $r_2 = r_3 = \frac{2}{3}$	$r_1 = r_2 = \frac{1}{23}$ $r_3 = \frac{126}{23}$
T_{ij}	$T_{12} = T_{13} = 1$ $T_{21} = T_{31} = \frac{1}{2}$ $T_{23} = T_{32} = 0$	$T_{12} = T_{13} = \frac{2}{3}$ $T_{21} = T_{31} = \frac{1}{2}$ $T_{23} = T_{32} = \frac{1}{3}$	$T_{12} = T_{21} = \frac{11}{12}$ $T_{31} = T_{32} = \frac{1}{12}$ $T_{13} = T_{23} = \frac{1}{2}$

that $r_k = R_k - (X_i//X_j)$. From (8c) and the input-matching condition at port k, we have

$$s_{ij} = [(R_i + R_j)R_k - R_iR_j]/2R_kB_{ij}. \tag{9}$$

Thus, when the load resistors are given, the resistively matched three-port can be realized by using (8) and (9).

Next, let us consider the regions where $r_1, r_2, r_3 \geq 0$. The horizontal and vertical axes in Fig. 2 are $A_{12}^2 = R_2/R_1$ and $A_{13}^2 = R_3/R_1$, respectively [13]. Two cases are of interest:

For $A_{12} \geq 1$:

$$3A_{12}/\Delta_a \leq R_3/R_1 \leq A_{12}/(A_{21} - A_{12} + 2\sqrt{A_{12}^2 - 1}) \tag{10a}$$

For $A_{12} \leq 1$:

$$3A_{12}/\Delta_a \leq R_3/R_1 \leq A_{12}/(A_{12} - A_{21} + 2\sqrt{A_{21}^2 - 1}) \tag{10b}$$

where $\Delta_a = A_{12} + A_{21} + 2\sqrt{A_{12}^2 + A_{21}^2 - 1}$.

The curves a, b, and c in Fig. 2 represent the cases of $r_1 = 0, r_2 = 0$, and $r_3 = 0$, respectively. The clear area inside these three curves is the region where $r_1, r_2, r_3 \geq 0$. The hatched area indicates the region where $0 < s_{12}, s_{13}, s_{23} < 1$ and one of the three resistors r_1, r_2, and r_3 becomes negative. Table I shows numerical examples of this, which will be discussed later.

III. SERIES EXPANSIONS AND THEIR NETWORK TRANSFER FUNCTIONS

Let us consider the network shown in Fig. 3. Although arbitrary branching resistors r_i are assumed here, if the results from Section II are applied to them, no reflections can be expected at the junction of the three lines. The symbols in Fig. 3 are as follows:

R_{1s} is the internal resistance of the source;
R_{2l}, R_{3l} are resistors for input matching or amplitude compensation in high-input-impedance logical circuits; and
z_1, z_2, z_3 are the characteristic impedances of lines 1, 2, and 3, respectively.

Fig. 4 shows an equivalent signal-flow graph (SFG), where each line in Fig. 3 is divided into two parts: the upper and lower lines on which the forward and backward traveling waves, respectively, propagate. τ_i is the time required for the TEM wave to propagate on the ith line. T_1 is the voltage-transmission coefficient from the generator to line 1. In Fig. 4, Γ_{ii} and T_{ij} are given by replacing R_i in (2) with z_i. T_1 and Γ_i are given by

$$\begin{aligned} T_1 &= z_1/(R_{1s} + z_1) \\ \Gamma_1 &= (R_{1s} - z_1)/(R_{1s} + z_1) \\ \Gamma_i &= (R_{il} - z_i)/(R_{il} + z_i), i = 2, 3. \end{aligned} \tag{11}$$

$1 + \Gamma_i$ represents the voltage-transmission coefficient from line i to the load R_{il}. When an incident wave is applied to port i_c $(i = 1, 2, 3)$, the characteristic impedances in Fig. 3 play the same role as the load resistors in Fig. 1, because the incident wave cannot see the terminal resistors R_{1s}, R_{2l}, and R_{3l} at this point. Replacing R_i in (3) through (9) with z_i enables the resistively matched three-port in Fig. 1 to be realized at the junction in Fig. 3.

As transmission lines of unequal length are used in Fig. 3, the network transfer functions will include three different variables:

$$\xi_i = \exp(-s\tau_i), s = j\omega, i = 1, 2, 3. \tag{12}$$

When w_{1k-1} travels from port 1_c to port 1, is reflected at port 1, and then arrives again at port 1_c, we have $u_{1k} = \Gamma_i\xi_1^2 w_{1k-1}$. Therefore,

$$\boldsymbol{u}_k = \begin{bmatrix} \Gamma_1\xi_1^2 & 0 & 0 \\ 0 & \Gamma_2\xi_2^2 & 0 \\ 0 & 0 & \Gamma_3\xi_3^2 \end{bmatrix} \boldsymbol{w}_{k-1}. \tag{13}$$

Denoting the above matrix by $[\boldsymbol{D}]$, and using (1), we obtain

$$\boldsymbol{w}_k = \boldsymbol{\Gamma}_\xi \boldsymbol{w}_{k-1} = \boldsymbol{\Gamma}_\xi^{k-1} \boldsymbol{w}_1 \tag{14}$$

where $\boldsymbol{\Gamma}_\xi = [\boldsymbol{T}][\boldsymbol{D}]$. When a forward-traveling voltage wave $\delta(t)$ appears at port 1, and as $\xi_1 = \mathcal{F}[\delta(t - \tau_1)]$ at port 1_c, the initial condition can be given by

$$\boldsymbol{u}_1 = [\xi_1 \quad 0 \quad 0]^t \tag{15}$$

where $\mathcal{F}$ is the Fourier transform and t denotes transpose. Therefore,

$$\boldsymbol{w}_1 = [\boldsymbol{T}]\boldsymbol{u}_1 \tag{16}$$

The true voltages w_{ob1}, w_{ob2}, and w_{ob3} that are induced by $\boldsymbol{w}_k$ at ports 1, 2, and 3 are obtained as the sum of the incident

and reflected voltage waves [16]. Therefore,

$$\boldsymbol{w}_{ob} = \begin{bmatrix} (1+\Gamma_1)\xi_1 & 0 & 0 \\ 0 & (1+\Gamma_2)\xi_2 & 0 \\ 0 & 0 & (1+\Gamma_3)\xi_3 \end{bmatrix} \boldsymbol{w}_k \quad (17)$$

where $\boldsymbol{w}_{ob} = [w_{ob1} \quad w_{ob2} \quad w_{ob3}]^t$. Denoting the above matrix by $[\boldsymbol{N}]$, and using (14), we obtain the sum total for $\boldsymbol{w}_{ob}$ for $k = 1, 2, \ldots$, which can be represented by

$$\boldsymbol{G}(\xi_i) = [\boldsymbol{N}](\boldsymbol{E} + \boldsymbol{\Gamma}_\xi + \boldsymbol{\Gamma}_\xi^2 + \cdots)\boldsymbol{w}_1 \quad (18)$$

where $\boldsymbol{G}(\xi_i) = [G_{11}(\xi_i)\, G_{12}(\xi_i)\, G_{13}(\xi_i)]^t$. The element $G_{11}(\xi_i)$ must be equal to the reflection coefficient "seen" looking into the network in Fig. 3 from port 1, and the other elements $G_{12}(\xi_i)$ and $G_{13}(\xi_i)$ must represent the network transfer functions from port 1 to port $i, i = 2, 3$, because the input of $\delta(t)$ is assumed at first, after which the components of the output response are all added at each output port. In calculating (18) up to $k = 3$, for instance, $G_{12}(\xi_i)$ is given by

$$\begin{aligned} G_{12}(\xi_i) = {} & (1+\Gamma_2)\xi_1\xi_2\{T_{12} + (T_{13}\Gamma_3 T_{32}\xi_3^2 \\ & + \Gamma_{11}\Gamma_1 T_{12}\xi_1^2 + T_{12}\Gamma_2\Gamma_{22}\xi_2^2) \\ & + [(\Gamma_{11}\Gamma_1)^2 T_{12}\xi_1^4 + \Gamma_{11}\Gamma_1 T_{12}\Gamma_2\Gamma_{22}\xi_1^2\xi_2^2 \\ & + (\Gamma_{11}\Gamma_1 T_{13}\Gamma_3 T_{32} + T_{13}\Gamma_3 T_{31}\Gamma_1 T_{12})\xi_1^2\xi_3^2 \\ & + T_{12}\Gamma_2 T_{21}\Gamma_1 T_{12}\xi_2^2\xi_1^2 + T_{12}(\Gamma_2\Gamma_{22})^2\xi_2^4 \\ & + (T_{13}\Gamma_3 T_{32}\Gamma_2\Gamma_{22} + T_{12}\Gamma_2 T_{23}\Gamma_3 T_{32})\xi_3^2\xi_2^2 \\ & + T_{13}\Gamma_3\Gamma_{33}\Gamma_3 T_{32}\xi_3^4] + \ldots\} \end{aligned} \quad (19)$$

The first component of (19) represents the first arriving wave. Equation (18) can now be rewritten as (see Appendix A)

$$\boldsymbol{G}(\xi_i) = [\boldsymbol{N}](\boldsymbol{E} - \boldsymbol{\Gamma}_\xi)^{-1}\boldsymbol{w}_1. \quad (20)$$

In calculating the inverse matrix, the transfer function $G_{12}(\xi_i)$ is given by

$$\begin{aligned} G_{12}(\xi_i) = {} & \{(1+\Gamma_2)\xi_1\xi_2[T_{12} \\ & + (T_{13}T_{32} - T_{12}\Gamma_{33})\Gamma_3\xi_3^2]\}/\Delta \end{aligned} \quad (21)$$

where Δ is given by the following:

$$\begin{aligned} \Delta = {} & 1 - \Gamma_1\Gamma_{11}\xi_1^2 - \Gamma_2\Gamma_{22}\xi_2^2 - \Gamma_3\Gamma_{33}\xi_3^2 \\ & + [(\Gamma_{11}\Gamma_{22} - T_{12}T_{21})\Gamma_1\Gamma_2]\xi_1^2\xi_2^2 \\ & + [(\Gamma_{22}\Gamma_{33} - T_{23}T_{32})\Gamma_2\Gamma_3]\xi_2^2\xi_3^2 \\ & + [(\Gamma_{11}\Gamma_{33} - T_{13}T_{31})\Gamma_1\Gamma_3]\xi_1^2\xi_3^2 \\ & + [(\Gamma_{11}T_{23}T_{32} + \Gamma_{22}T_{13}T_{31} + \Gamma_{33}T_{12}T_{21} \\ & - \Gamma_{11}\Gamma_{22}\Gamma_{33} - T_{12}T_{23}T_{31} - T_{13}T_{32}T_{21}) \\ & \bullet \Gamma_1\Gamma_2\Gamma_3]\xi_1^2\xi_2^2\xi_3^2 \end{aligned}$$

IV. The Characteristic of Output Responses

A. The Sum of Impulse Response Components

As we can see from (19), the coefficients of the expansion provide the impulse response components directly. As $\xi_{i|\omega=0} = 1$, the sum of all the network's impulse response components can be given by the following:

$$\begin{aligned} & G_{12}(\xi_i)_{|\omega=0} \\ & \quad = \{(1+\Gamma_2)[T_{12} + (T_{13}T_{32} - T_{12}\Gamma_{33})\Gamma_3]\}/\Delta_{|\omega=0} \end{aligned} \quad (22)$$

From the convolution [6], [9], the step responses (or ramp responses) are obtained by adding the replicas of the applied waveform according to the time spacings given by the ξ_i's. Therefore, the amplitude at the steady state for an input unit function can also be obtained from (22). Equation (22) is necessary if one is to study the relationship of the first arriving wave to the steady state (see Fig. 12, below).

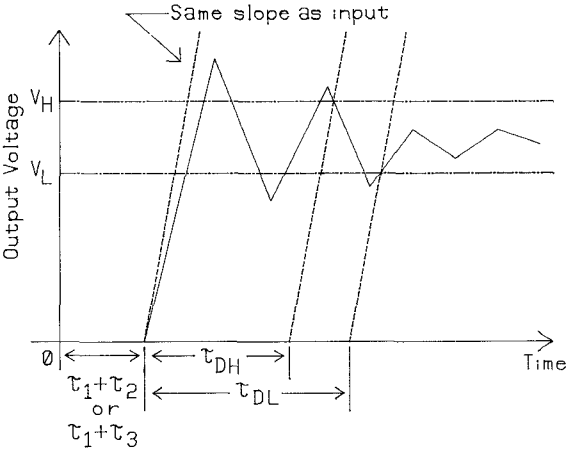

Fig. 5. Graphic definition of the effective delay time $\tau_d = \max(\tau_{DH}, \tau_{DL})$.

B. The Monotonic Increment of Output Responses

From (2b), $T_{ij} \geq 0$ holds for non-negative resistors. Therefore, under the conditions of $\Gamma_i, \Gamma_{ii} \geq 0$, the impulse-response components are always positive and the output waveforms for an input step function increase monotonically.

C. The Effective Delay Time τ_D

Let us introduce threshold levels V_L and V_H. For instance, $V_L = 0.9$ and $V_H = 1.1$ could be set as a tolerance for the high level 1.0. In this paper the effective delay time τ_D is defined by $\tau_D = \max(\tau_{DH}, \tau_{DL})$ (from Fig. 5). τ_{DL} is the period from the onset of an output waveform to the time at which the output response rises past the lower threshold level V_L (and never falls below V_L after that). τ_{DH} is defined similarly for the upper limit.

In the case of matched three-ports, $\Gamma_{ii} = 0$ holds for $i = 1, 2, 3$. Let the first arriving voltages at two output ports be

$$(1+\Gamma_2)T_{12}, (1+\Gamma_3)T_{13} \geq V_L. \quad (23)$$

If $\Gamma_i \geq 0$, then the output responses of an input step function increase monotonically and never fall below the first-stage threshold level V_L. Therefore, $\tau_D = 0$ holds if the steady-state values are within the range of tolerance.

TABLE II
AN EXPLANATION OF FIG. 7

	Normalized Element Values, $i=1,2,3$	Reflection Coefficients at the Junction	Input/Output Terminal Conditions	First Arriving Voltage	Steady-State Voltage	Monotonic Increment	Tolerance (0.9-1.1)	Illustration of Network Pattern
Case A (- - - - -)	$z_i = 1$ $r_i = 0$	$\Gamma_u = -\frac{1}{3}$	$\Gamma_1 = 0$[1] $\Gamma_2 = \Gamma_3 = 1$[2]	4/3	2	no	no[3] ($\tau_D \neq 0$)	no
Case B (———)	$z_i = 1$ $r_i = 0$	$\Gamma_u = -\frac{1}{3}$	$\Gamma_1 = \Gamma_2 = \Gamma_3 = 0$	2/3	2/3	yes[4]	no ($\tau_D \neq 0$)	no
Case C (— — —)	$z_i = 1$ $r_i = 0$	$\Gamma_u = -\frac{1}{3}$	$\Gamma_1 = 0$ $\Gamma_2 = \Gamma_3 = \frac{7}{20}$	0.9	1.02	no	no[5] ($\tau_D \neq 0$)	Fig. 9
Case D[6] (— —)	$z_1 = 1$ $z_2 = z_3 = \frac{4}{3}$ $r_1 = 0$ $r_2 = r_3 = \frac{2}{3}$	$\Gamma_u = 0$	$\Gamma_1 = 0$ $\Gamma_2 = \Gamma_3 = \frac{7}{20}$	0.9	1.02	yes	yes[7] ($\tau_D = 0$)	Fig. 10(a)

Notes to Table II: (1) Input match. (2) Open terminals. (3) τ_D = effective delay time. (4) The amplitudes are constantly 2/3 for $G_{12}(\xi_i) = (\frac{2}{3})\xi_1\xi_2$ and $G_{13}(\xi_i) = (\frac{2}{3})\xi_1\xi_3$. (5) The network transfer functions for this case are as follows:

$$G_{12}(\xi_i) = (\tfrac{9}{10})\xi_1\xi_2 - (\tfrac{21}{100})\xi_1\xi_2^3 + (\tfrac{21}{100})\xi_1\xi_2\xi_3^2 + \cdots$$
$$G_{13}(\xi_i) = (\tfrac{9}{10})\xi_1\xi_3 + (\tfrac{21}{100})\xi_1\xi_2^2\xi_3 - (\tfrac{21}{100})\xi_1\xi_3^3 - \cdots$$

The tolerance is satisfied neither at port 2 nor at port 3 by the second terms. After the third terms, the output responses satisfy the tolerance. Comparing Case B with Case C, it is seen that the mismatch at ports 2 and 3 lifts the steady-state voltage from 2/3 to 1.02, and terminal resistors R_{2l} and R_{3l} of 27/13 in Fig. 9 contribute to amplitude compensation. (6) Case D is derived from point M. (7) The first arriving voltage 0.9, the steady-state voltage 1.02, and the monotonic increment, are independent of the length of the transmission line. Therefore, $\tau_D = 0$ holds, regardless of the variation of τ_1, τ_2, and τ_3.

V. NETWORKS FOR IDEAL RESPONSES

Fig. 6 shows an input ramp waveform. Figs. 7 and 8 show the results of output calculations where $\tau_1 = \tau_2 = 1.0$ nsec, $\tau_3 = 1.5$ nsec; $\Gamma_1 = 0$ is assumed. (The last two figures are constructed simply by adding replicas of Fig. 6; for further explanation of Figs. 7 and 8, refer to Tables II and III.) Fig. 9 shows a network with no branching resistors, representing Case C.

In the following we discuss cases where two characteristic impedances are equal. Matched three-ports at the junction are assumed.

A. For $z_2 = z_3$: The realization region is on the line representing $R_3/R_1 = R_2/R_1$ in Fig. 2. (In Fig. 3, R_3/R_1 and R_2/R_1 are replaced by z_3/z_1 and z_2/z_1.)

A.1. Point S of Fig. 2: From the T_{ij}'s in Table I and the SFG in Fig. 4, we have

$$G_{12}(\xi_i) = (1 + \Gamma_2)\xi_1\xi_2$$
$$\text{and } G_{13}(\xi_i) = (1 + \Gamma_3)\xi_1\xi_3$$

This indicates that the same waveform as an input can be obtained at two output ports. However, a negative branching resistor is required, as shown in Table I.

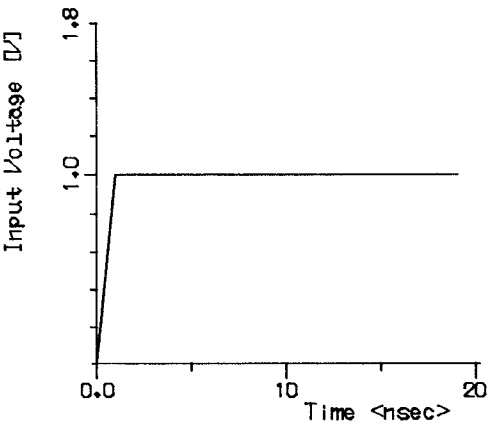

Fig. 6. An input ramp waveform.

A.2. Point M of Fig. 2: Point M is as near as possible to the ideal point S, providing an optimum three-port [13]. (For details, refer to Case D in Table II and Figs. 7 and 10(a)).

B. For $z_1 = z_2$: The realization region is on the line representing $z_2/z_1 = 1$ (i.e., on the line representing $R_2/R_1 = 1$ in Fig. 2). The realization region of the non-negative branching resistors is above the region defined by $0.75 \leq z_3/z_1 < \infty$.

TABLE III
AN EXPLANATION OF FIG. 8(1)

	Normalized Element Values	Reflection Coefficients at the Junction	Input/Output Terminal Conditions	First Arriving Voltage	Steady-State Voltage	Monotonic Increment	Tolerance (0.9-1.1)	Illustration of Network Pattern
Case AA (- - - -)	$z_1 = z_2 = 1$ $z_3 = 6$ $r_1 = r_2 = \frac{1}{23}$ $r_3 = \frac{126}{23}$	$\Gamma_{ii} = 0$	$\Gamma_1 = 0$ $\Gamma_2 = -\frac{1}{55}$ $\Gamma_3 = \frac{4}{5}$	0.9	0.932(2) 0.884(3)	no(4)	no(5) ($\tau_D \neq 0$)	no
Case BB (——)	$z_1 = z_2 = 1$ $z_3 = 6$ $r_1 = r_2 = \frac{1}{23}$ $r_3 = \frac{126}{23}$	$\Gamma_{ii} = 0$	$\Gamma_1 = 0$ $\Gamma_2 = \frac{1}{22}$ $\Gamma_3 = \frac{11}{12}$	23/24(6)	1.0	yes	yes ($\tau_D = 0$)	Fig. 10(b)
Case CC (— - — -)	$z_1 = z_2 = 1$ $z_3 = 6$ $r_1 = r_2 = 0$(7) $r_3 = \frac{126}{23}$	$\Gamma_{11} = -\frac{23}{551}$(7) $\Gamma_{22} = -\frac{23}{551}$ $\Gamma_{33} = -\frac{1}{551}$	$\Gamma_1 = 0$ $\Gamma_2 = \frac{1}{550}$ $\Gamma_3 = \frac{527}{575}$	0.96	0.998(2) 0.960(3)	no(8)	yes(9) ($\tau_D = 0$)	no

Notes to Table III: (1) Cases AA, BB, and CC are derived from point Q. (2) Value at port 2. (3) Value at port 3. (4), (5) These are because $\Gamma_2 < 0$. To be $\Gamma_2 \geq 0$, the first arriving voltage $(1 + \Gamma_2)T_{12}$ must be greater than or equal to 0.917. (6) The value 23/24 is found at the intersection of two curves, drawn with a solid line, in Fig. 12. (7) As r_1 and r_2, derived from point Q, have the low resistance 1/23, they are removed. Therefore, $\Gamma_{ii} \neq 0$, $i = 1.2.3$. (8), (9) The conditions for monotonic increment are not satisfied. However, the upward and downward vibrations due to $\Gamma_{ii} < 0$ are not easily observed in Figs. 8(a) and (b). In Fig. 8(a) the output response at port 2 is virtually the same as that in Case BB.

From $z_1 = z_2$ we have

$$T_{12} = T_{21} = (2z_3 - z_1)/(2z_3),$$
$$T_{31} = T_{32} = z_1/2z_3,$$
$$\text{and } T_{13} = T_{23} = 0.5$$

B.1. $z_3 \to \infty$: As $T_{12} = T_{21} \to 1, T_{31} = T_{32} \to 0$, and $T_{13} = T_{23} \to 0.5$, then

$$G_{12}(\xi_i) \to (1 + \Gamma_2)\xi_1\xi_2$$
$$\text{and } G_{13}(\xi_i) \to 0.5(1 + \Gamma_3)\xi_1\xi_3(1 + \Gamma_2\xi_2^2)$$

As $\Gamma_2 = 0$ and $\Gamma_3 = 1$, ideal results are obtained as in the case of point S. However, a transmission line havig $z_3 = \infty$ cannot be fabricated in a practical application. Therefore, point Q of Fig. 2, i.e., where $z_3/z_1 = 6$ (this is 300Ω for the reference impedance of 50Ω), will be chosen as a value that can be realized.

B.2. Point Q of Fig. 2: Point Q offers desirable results in a different sense than does point M. Figure 10(b) indicates one of the networks designed from point Q. (For details, refer to Fig. 8 and Table III.)

VI. The Amplitudes of the First Arriving Wave That Are Required for Tolerance

As shown in Case AA of Table III, even if the first arriving wave satisfies the tolerance range from 0.9 to 1.1, the steady-state voltage does not always satisfy that condition. Therefore, it is necessary to examine the relationship of the first arriving voltage (FAV) to the reflection coefficients Γ_2 and Γ_3, as well as to the steady-state voltage. Let us now consider two cases, referring to Figs. 11 and 12.

A. Point M (dashed line): $\Gamma_i \geq 0, i = 1, 2, 3$ holds in the range $0.9 \leq \text{FAV} \leq 1.1$.

The steady-state voltage in the range 0.9 to 1.1 is satisfied by $0.9 \leq \text{FAV} \leq 0.946$.

B. Point Q (solid line):

$$\Gamma_i \geq 0 \text{ for } 0.917 \leq \text{FAV} \leq 1.1,$$

The steady-state voltage in the range 0.9 to 1.1 is satisfied by $0.908 \leq \text{FAV} \leq 1.006$.

For the above two cases it can be seen that FAV has to be set in the range from 0.9 to 0.946 for the networks derived from point M, and in the range from 0.917 to 1.006 for the networks derived from point Q, in order to satisfy the monotonic increment, the given tolerance range (0.9-1.1), and $\tau_D = 0$.

Considering the tolerance range of FAV, it can be said that the realizability of output waveforms such as those in cases D of Table II and BB of Table III is limited to a narrow region.

VII. Power Dissipation

Let us assume that an impulse voltage wave of unit amplitude is applied to port 1 at $t = 0$. From $z_1 = 1$, the

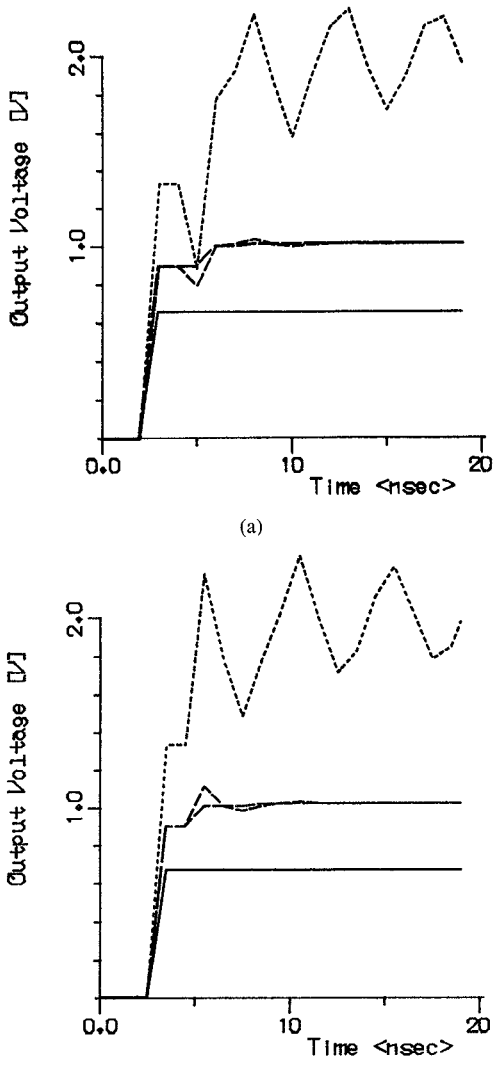

Fig. 7. Output waveforms. (a) At port 2. (b) At port 3. Case A: – – –; Case B: ——; Case C: – – –; Case D — —

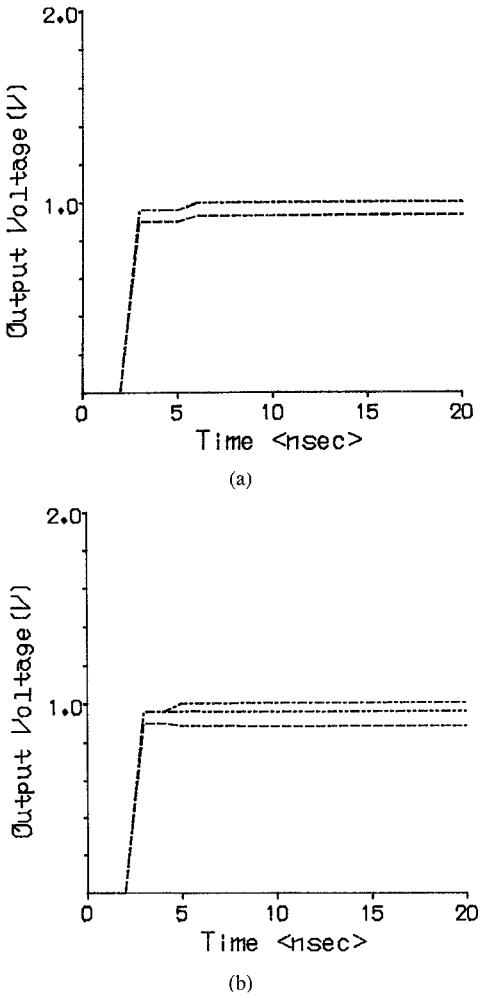

Fig. 8. Output waveforms. (a) At port 2. (b) At port 3. Case AA: ——; Case BB: – – –; Case CC: – – – –

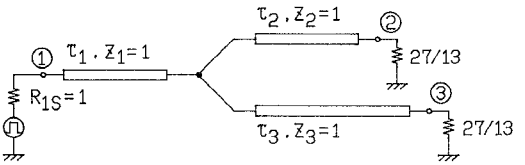

Fig. 9. A network with no branching resistors, representing Case C

incident power is represented by $P_{in} = 1$ (see Appendix B). In this section the output waveforms derived from the network impulse components through convolution [6], [9] are assumed not to overlap.

A. Power Dissipation at Terminals

The power P_{sr}, to be returned to the source, and the powers P_{o2} and P_{o3}, to be consumed at ports 2 and 3, are represented by

$$P_{sr} = G_{1s} \sum_{k=1}^{\infty} A_{rk}^2 \tag{24a}$$

and

$$P_{oi} = G_{il} \sum_{k=1}^{\infty} A_{ik}^2 \tag{24b}$$

where $G_{1s} = 1/R_{1s}$ and $G_{il} = 1/R_{il}, i = 2, 3$. A_{rk} and $A_{ik}, i = 2, 3$, are the kth expansion coefficients of $G_{11}(\xi_i), G_{12}(\xi_i)$, and $G_{13}(\xi_i)$, respectively.

B. Power Losses in the Inner Resistors

B.1. Power Loss $P_d(\tau_1)$: When a unit incident power $P_{in} = 1$ arrives at port 1_c at time $t = \tau_1$, let the power transmitted from port 1_c to port 2_c be $P(2_c, \tau_1) = |S_{12}|^2$, and let that from port 1_c to port 3_c be $P(3_c, \tau_1) = |S_{13}|^2$. As the reflected power at port 1_c is given by $|S_{11}|^2$, the power loss $P_d(\tau_1)$ at $t = \tau_1$ is represented by

$$P_d(\tau_1) = (1 - |S_{11}|^2 - |S_{12}|^2 - |S_{13}|^2). \tag{25}$$

B.2. Power Losses $P_d(\tau_1 + 2\tau_2), P_d(\tau_1 + 2\tau_3)$: The reflected power at port 2 at $t = \tau_1 + \tau_2$ is $P(2, \tau_1 + \tau_2) = |\Gamma_2|^2 P(2_c, \tau_1)$. When the reflected voltage wave at port 2 is transmitted from port 2_c to ports 1_c and 3_c at $t = \tau_1 + 2\tau_2$, the power loss

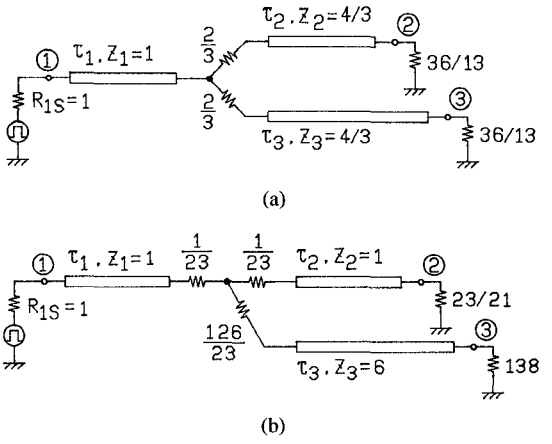

Fig. 10. Networks including resistively matched three-ports. (a) A network designed from point M, representing Case D. (b) A network designed from point Q, representing Case BB.

$P_d(\tau_1 + 2\tau_2)$ is represented by

$$P_d(\tau_1 + 2\tau_2) = P(2, \tau_1 + \tau_2)(1 - |S_{22}|^2 - |S_{12}|^2 - |S_{23}|^2). \tag{26}$$

Similarly, the power loss at time $t = \tau_1 + 2\tau_3$ is represented by

$$P_d(\tau_1+2\tau_3) = P(3, \tau_1+\tau_3)(1-|S_{33}|^2-|S_{13}|^2-|S_{23}|^2) \tag{27}$$

where $P(3, \tau_1 + \tau_3) = |\Gamma_3|^2 P(3_c, \tau_1). |S_{22}|^2$ and $|S_{33}|^2$ relate to the reflected power at ports 2c and 3c, respectively.

C. A Numerical Example for Fig. 10(b)

The following are the results of calculations up to the third component:

$$G_{11}(\xi_i) = \xi_1^2(11\xi_2^2/288 + 11\xi_3^2/288 + 11\xi_2^2\xi_3^2/3456 + \ldots)$$
$$G_{12}(\xi_i) = \xi_1(23\xi_2/24 + 23\xi_3^2\xi_2/576 + 23\xi_3^2\xi_2^3/13824 + \ldots)$$
$$G_{13}(\xi_i) = \xi_1(23\xi_3/24 + 23\xi_2^2\xi_3/576 + 23\xi_2^2\xi_3^3/13824 + \ldots)$$

From Section VII-A, the power dissipations at ports 1, 2, and 3 are, respectively.

$$P_{sr} = 0.002928,$$
$$P_{o2} = 0.840000,$$
$$\text{and } P_{o3} = 0.006667$$

The scattering matrix derived from (3) is

$$\boldsymbol{S} = \begin{bmatrix} 0 & \frac{11}{12} & \frac{\sqrt{6}}{12} \\ \frac{11}{12} & 0 & \frac{\sqrt{6}}{12} \\ \frac{\sqrt{6}}{12} & \frac{\sqrt{6}}{12} & 0 \end{bmatrix}.$$

From Section VII-B, we calculate the power losses of the inner resistors as

$$P_d(\tau_1) = 0.118056,$$
$$P_d(\tau_1 + 2\tau_2) = 0.000205,$$
$$\text{and } P_d(\tau_1 + 2\tau_3) = 0.032094.$$

The resultant total power dissipation P_{dt} is 0.99995.

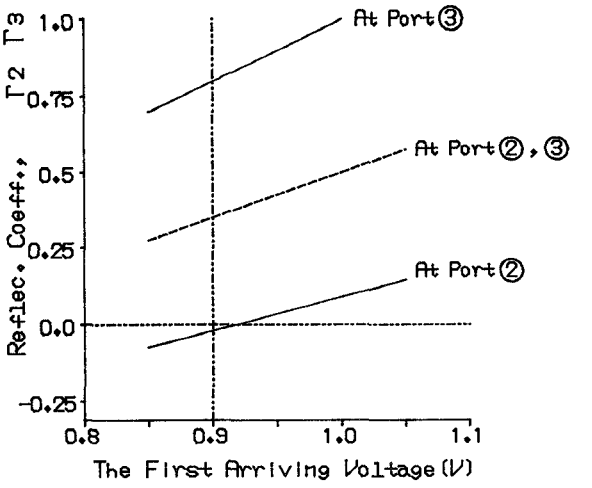

Fig. 11. Γ_2 and Γ_3 versus the first arriving voltage. – – –: Networks derived from point M. ——; Networks derived from point Q.

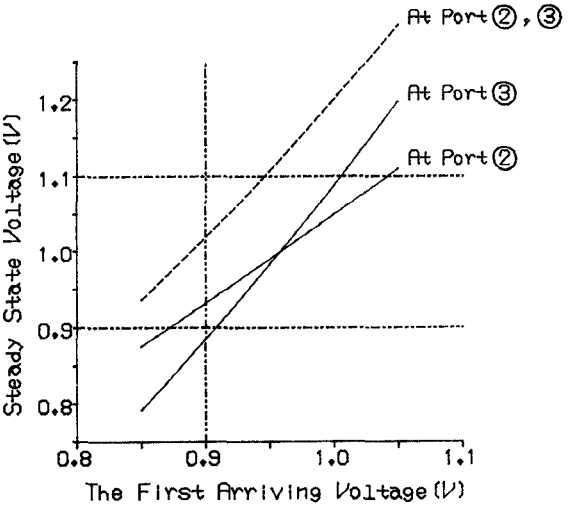

Fig. 12. Steady-state voltage versus the first arriving voltage. – – –: Networks derived from point M. ——: Networks derived from point Q.

VIII. Conclusion

The expansions of network transfer functions involving three variables have been used to calculate the output responses of three-port networks consisting of three transmission lines and three branching resistors at a junction. These calculations are useful in the analysis of multiple reflections and network design where the interconnections of high-speed logic circuits [3], [11] or computer networks [12] are concerned. A well-known method, that of the lattice diagram [4], is often used to achieve the same analysis and design goals. However, with the method of expansion presented here, each term corresponds to an individual reflection, i.e., the first arriving wave, the second arriving wave, and so forth. It is expected that this series-expansion approach will be easier to apply than the lattice diagram method.

The proposed networks are found to be useful not only for dividing input signals without producing reflections, but also for increasing the speed of logic circuits, because the given tolerances of output amplitudes can be satisfied from

the beginning and there is no effective time delay. The results presented here can be confirmed as follows. Equation (19) can also be obtained by tracing all possible paths in Fig. 4. The network transfer function in (21) is equal to a result derived from Mason's formula [17]. Also, Case B is a familiar empirical case. The calculations of power dissipation include no contradiction.

In this paper, lossless transmission lines, TEM wave propagation, and pure resistances have been assumed. With regard to the resistors, their physical dimensions have been ignored, as is usual in electric circuit theory [15], because the propagation-delay times for the resistors are short enough compared with those for the lines in interconnections. Even if the parallel capacitances are included in the terminal resistors of Fig. 3, these capacitive components will disappear in the steady state, and thus the output transient responses will asymptotically approach those of a network consisting of pure resistances. Given this fact and the above assumptions, it can be said that the fundamental behavior of the three-port transmission-line network has been investigated.

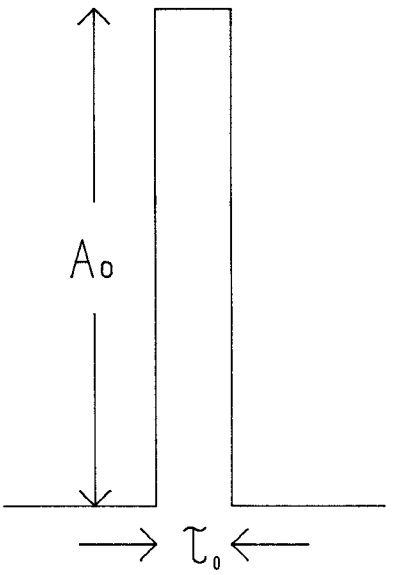

Fig. 13. A rectangular wave.

IX. Appendix A
The Convergence of Γ_ξ

Rewriting (3), we obtain $[\boldsymbol{T}] = [\sqrt{\boldsymbol{z}}][\boldsymbol{S}][\sqrt{\boldsymbol{z}}]^{-1}$ for the resistive three-port of Fig. 3, where $[\sqrt{\boldsymbol{z}}] = \text{diag}\,[\sqrt{z_1}, \sqrt{z_2}, \sqrt{z_3},]$. $T_{ij} > 1$ is satisfied in some cases, so the convergence of $\boldsymbol{\Gamma}_\xi$ is of interest:

$$\boldsymbol{\Gamma}_\xi^k = ([\boldsymbol{T}][\boldsymbol{D}])^k = [\sqrt{\boldsymbol{z}}][\boldsymbol{S}]([\boldsymbol{D}][\boldsymbol{S}])^{k-1}[\sqrt{\boldsymbol{z}}]^{-1}[\boldsymbol{D}] \quad \text{(A1)}$$

For a passive network such as that in Fig. 1, we obtain

$$P_d = [\boldsymbol{a}]^+[\boldsymbol{a}] - ([\boldsymbol{S}][\boldsymbol{a}])^+([\boldsymbol{S}][\boldsymbol{a}]) \geq 0 \quad \text{(A2)}$$

where "+" indicates a conjugate transpose and $[\boldsymbol{a}] = [a_1 \quad a_2 \quad a_3]^t \neq [0]$. Equation (A2) holds for all complex values of a_i, $i = 1, 2, 3$ [16]. When $[\boldsymbol{A}] = [\boldsymbol{D}][\boldsymbol{S}]$,

$$\begin{aligned}&([\boldsymbol{S}][\boldsymbol{a}])^+([\boldsymbol{S}][\boldsymbol{a}]) - ([\boldsymbol{A}][\boldsymbol{a}])^+([\boldsymbol{A}][\boldsymbol{a}])\\ &\quad = ([\boldsymbol{S}][\boldsymbol{a}])^+\boldsymbol{Q}_0([\boldsymbol{S}][\boldsymbol{a}]) > 0 \end{aligned} \quad \text{(A3)}$$

where $\boldsymbol{Q}_0 = \text{diag}\,(1 - |\Gamma_i|^2)$. From (A2) we obtain

$$P_d = [\boldsymbol{a}]^+[\boldsymbol{a}] - ([\boldsymbol{A}][\boldsymbol{a}])^+([\boldsymbol{A}][\boldsymbol{a}]) > 0 \quad \text{(A4)}$$

Let the eigenvalue and eigenvector of $[\boldsymbol{A}]$ be α and $[\boldsymbol{x}]$. From $[\boldsymbol{A}][\boldsymbol{x}] = \alpha[\boldsymbol{x}]$ and (A4), we obtain

$$[\boldsymbol{x}]^+[\boldsymbol{x}] - ([\boldsymbol{A}][\boldsymbol{x}])^+([\boldsymbol{A}][\boldsymbol{x}]) = (1 - |\alpha|^2)[\boldsymbol{x}]^+[\boldsymbol{x}] > 0 \quad \text{(A5)}$$

Therefore, $|\alpha|^2 < 1$. From (A1), this condition is equivalent to $\boldsymbol{\Gamma}_\xi^k \to 0\,(k \to \infty)$. Therefore, (20) can be derived from (18).

X. Appendix B
Power Dissipation

When a rectangular wave such as that shown in Fig. 13 is applied to a conductance G_0, the consumed energy will be $W_0 = G_0 A_0^2 \tau_0$. Let us assume that this rectangular wave is applied to port 1 in Fig. 3. As pointed out in the summary of [6], the time response consists of replicas of the applied pulse, with each replica having an amplitude A_k that is given by the coefficient of a term in the network impulse responses. When one of these replicas is incident to a load G_l, the consumed energy will be $W_l = G_l A_k^2 \tau_0$. When $G_0 = 1$ and $A_0 = 1$, the ratio W_l/W_0 becomes equal to $G_l A_k^2$, and hence represents the ratio of the power consumption at the load to the incident unit power.

References

[1] H. A. Wheeler, "The interpretation of amplitude and phase distortion in terms of paired echoes," *Proc. IRE*, vol. 27, pp. 359–385, June 1939.
[2] K. Ohue, "Constant-resistance phase equalizers using directional couplers, *Trans. IECE Japan*, vol. J63-B, no. 5, pp. 460–467, 1980.
[3] M. Kato and I. Yosino, "Performance analysis in z- plane of branched transmission line with branching resistors," *Trans. IEICE Japan*, vol. J62-D, no. 5, pp. 317–324, 1979.
[4] *ECL Data Book*. chaps. 4–6, New York: Fairchild, 1977.
[5] C.-W. Hsue, "Elimination of ringing signals for a lossless, multiple-section transmission line," *IEEE Trans. Microwave Theory Tech.*, vol. 37, pp. 1178–1183, Aug. 1989.
[6] W. Getsinger, "Analysis of certain transmission-line networks in the time domain," *IRE Trans. Microwave Theory and Tech.*, vol. MTT-8, pp. 301–309, May 1960.
[7] G. F. Ross, "The transient analysis of certain TEM mode four-port networks," *IEEE Trans Microwave Theory and Tech.*, vol. MTT-14, pp. 528–542, Nov. 1966.
[8] K. A. Boakye and O. Wing, "On the analysis and realization of cascaded transmission-line networks in the time domain," *IEEE Trans. Circuit Theory*, vol. CT-20, pp. 301–307, May 1973.
[9] L. J. P. Linner, "Time domain analysis of commensurate distributed-line networks," *IEEE Trans. Circuits Syst.*, vol. CAS-22, pp. 334–343, Apr. 1975.
[10] C.-W. Hsue and C. D. Hechtman, "Transient analysis of nonuniform, high-pass transmission lines," *IEEE Trans. Microwave Theory Tech.*, vol. 38, pp. 1023–1030, Aug. 1990.
[11] D. A. Gradl, "Analysis of transmission-line signal distribution to multiple ports," *IEEE Trans. Circuits Syst.*, vol. CAS-29, pp. 270–272, Apr. 1982.
[12] C. W. Trueman, "An electromagnetic course with EMC applications for computer engineering students," *IEEE Trans. Educ.*, vol. E-33, pp. 119–128, Feb. 1990.
[13] I. Sakagami, "On suppression of multiple reflections by resistively matched 3-ports," in *Proc. 33rd Midwest Symp. on Circuits and Systems*, Aug. 1990, pp. 227–230.
[14] I. Sakagami and A. Kaji, "On the transmission of high-speed voltage waves at the junction of three transmission lines," in *Proc. SPIE, Int. Conf. on Advances in Interconnects and Packaging*, vol. 1389, Nov. 1990, pp. 329–339.

[15] C. A. Desoer and E. S. Kuh, *Basic Circuit Theory*. New York: McGraw-Hill, 1969, p. 2, pp. 734–738.
[16] H. J. Carlin and A. B. Giordano, *Network Theory: An Introduction to Reciprocal and Nonreciprocal Circuits* Englewood Cliffs, NJ: Prentice-Hall, 1964, Section 4.8.
[17] S. J. Masion, "Feedback theory–Some properties of signal flow graphs," *Proc. IRE*, vol. 41, pp. 1144–1156, Sept. 1953.

Iwata Sakagami (M'81) received the B.S., M.S., and Ph.D. degrees in electronic engineering from Hokkaido University, in 1972, 1977 and 1980, respectively.

From 1972 to 1974 he was with the Communication Equipment Works, Mitsubishi Electric Corp., Amagasaki-shi, Japan, where he was engaged in the development and design in microwave circuits and TV signal repeater systems. From 1980 to 1987 he was a Research Associate at the Research Institute of Applied Electricity, Hokkaido University. From 1987 to 1988 he was an Associate Professor at the Kushiro National Technical College. Since 1988 he has been an Associate Professor at the Muroran Institute of Technology. Dr. Sakagami is a member of IPSJ.

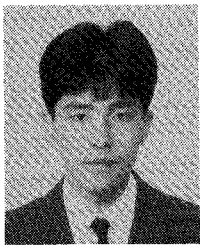

Akihiro Kaji received the B.E. and M.E. degrees in 1990 and 1992, respectively, both from the Muroran Institute of Technology, Muroran-shi, Japan. In 1992 he joined the Nippon Telegraph and Telephone Public Corporation, Iwamizawa-shi, Hokkaido, Japan.